THE UNIVERSITY OF WARWICK

warwickpublicationswrap

highlight your research

http://go.warwick.ac.uk/lib-publications

Intrinsic Electrochemical Activity of Single Walled Carbon Nanotube-Nafion Assemblies

Michael E. Snowden, Martin A. Edwards, Nicola C. Rudd, Julie. V. Macpherson, and Patrick R. Unwin[*]

Department of Chemistry, University of Warwick, Coventry, CV4 7AL, United Kingdom

[*]Email: p.r.unwin@warwick.ac.uk

Abstract

The intrinsic electrochemical properties and activity of single walled carbon nanotube (SWNT) network electrodes modified by a drop-cast Nafion film have been determined using the one electron oxidation of ferrocene trimethyl ammonium (FcTMA$^+$) as a model redox probe in the Nafion film. Facilitated by the very low transport coefficient of FcTMA$^+$ in Nafion (apparent diffusion coefficient of 1.8×10^{-10} cm^2 s^{-1}), SWNTs in the 2-D network behave as individual elements, at short (practical) times, each with their own characteristic diffusion, independent of neighbouring sites, and the response is diagnostic of the proportion of SWNTs active in the composite. Data are analysed using candidate models for cases where: (i) electron transfer events only occur at discrete sites along the sidewall (with a defect density typical of chemical vapour deposition SWNTs); (ii) all of the SWNTs in a network are active. The first case predicts currents that are much smaller than seen experimentally, indicating that significant portions of SWNTs are active in the SWNT/Nafion composite. However, the predictions for a fully active SWNT result in higher currents than seen experimentally, indicating that a fraction of SWNTs are not connected and/or that not all SWNTs are wetted completely by the Nafion film to provide full access of the redox mediator to the SWNT surface.

Introduction

Carbon nanotube (CNT)–polymer composites are attracting considerable attention as electrode materials for a diversity of electrochemical applications.[1-6] Among a wide range of materials, CNT–Nafion[1, 2, 7] modified electrodes have been investigated intensively,[1, 2, 7-9] with uses encompassing electroanalysis,[10, 11] the detection of neurotransmitters,[12, 13] as new composites for fuel cell proton exchange membranes,[14-16] and for electrocatalysis.[17-20] For all of these applications, improved knowledge of the underpinning physicochemical properties of CNT–Nafion composites is highly valuable to aid the rational design of electrochemical devices.

Nafion films have a long history of use for electrode modification,[21-28] with key effects being the strong permselectivity towards cations, *i.e.* the accumulation of cations,[29, 30] and barrier (protective) effects.[2, 31, 32] The accumulation of cations combined with barrier properties have been utilised for the detection of the neurotransmitter dopamine in the presence of ascorbic acid.[33-41] Nafion films have been employed on electrodes as drop-cast films,[42, 43] and by layer-by-layer deposition methodologies including the Langmuir-Blodgett[44, 45] and Langmuir-Schaefer[25, 46-48] techniques. These techniques have facilitated the co-deposition of Nafion, with a redox mediator pre-loaded within the film[29, 30] or with nano-materials immobilized within the film.[47, 49] In general, effective mass transport rates of solutes in Nafion films are usually greatly reduced compared to aqueous solutions.[30, 46, 50-52]

The incorporation of CNTs into Nafion films for electrochemical applications has been demonstrated successfully in several formats. Drop-cast Nafion-CNT films have been applied as bio-sensors,[33, 53, 54] as support electrodes for fuel cell catalysts,[15, 16] and for the detection of heavy metals.[10, 11] However, these studies have tended to focus on applications of the Nafion-modified CNT electrode rather than the

fundamental effect of the Nafion membrane on the electrochemical response of the CNTs. An alternative approach, which we use herein, is to deposit a Nafion film onto CNTs formed on an insulating (inert) support. 2D networks of single walled carbon nanotubes (SWNTs) synthesised on insulating Si/SiO$_2$ substrates have been shown to have a low non-Faradaic background signal making them the material of choice for many electroanalytical approaches.[55-59] These formats are particularly attractive for fundamental studies, as the electrochemical signal is due solely to the CNTs.[55, 56, 60, 61]

There is much interest in understanding the sites of heterogeneous electron transfer (ET) on the surface of CNTs.[62] A body of work has proposed that ET occurs only at the open ends of SWNTs and multi-walled carbon nanotubes (MWNTs),[63-65] and at edge plane-like sites on MWNTs.[66] However, these models of reactivity are typically derived from voltammetric studies performed on CNT dispersions or films cast onto a conductive support, which makes it difficult to distinguish the role of the CNTs independently of the support material.[63-66] On the other hand, work on pristine SWNTs synthesised by catalysed chemical vapour deposition (cCVD), have found ET at the side wall to be facile. Notably, a format comprising an individual SWNT on an insulating support as the electrode, where the ends were not exposed to solution, displayed fast ET,[55] as did alternative studies on individual SWNTs.[67] The same conclusion has been reached through studies of individual SWNTs on an insulating support addressed by a microcapillary,[68] and, more recently, scanning electrochemical cell microscopy (SECCM) studies of SWNT networks of the type used herein, demonstrated that high rates of ET were observed from the majority of sidewalls of SWNTs.[69]

Here, we report on a composite electrode comprising of a drop-cast Nafion film on a network of SWNTs synthesised by cCVD on an insulating Si/SiO$_2$ support. The

drop-cast film of Nafion was characterised to determine the apparent diffusion coefficient and concentration of ferrocenyl-methyltrimethyl ammonium (FcTMA$^+$) as a redox probe within the film. As demonstrated previously on highly oriented pyrolytic graphite (HOPG),[50] the low apparent diffusion coefficient leads to a spatial decoupling of characteristic active areas of the substrate electrode on the timescale of electrochemical measurements. This allows different models for possible sites of electrochemical activity at the Nafion-SWNT interface to be probed and identified.

Experimental

Electrode fabrication

Two working electrode materials were used: (i) a 25 µm diameter Pt disc ultramicroelectrode (UME) in an insulating glass sheath of diameter ~2.5 mm, created in house by sealing a 25 µm diameter Pt wire (99.9% Goodfellow) in a borosilicate capillary (Clark Electromedical Instruments);[70] (ii) 2D SWNT networks, which were synthesised directly onto 1 cm^2 Si/SiO$_2$ chips (IDB Technologies Ltd., U.K.) by cCVD using methanol as the carbon feedstock and ferritin to deliver the iron catalyst particles.[71] SWNT samples with a network density of 3 - 4 µm µm^{-2} (SWNT length/substrate area) were used, which was sufficient to ensure a continuous metallic network.[72] Electrical contact to the SWNTs was facilitated by the evaporation of a 10 nm Cr adhesion layer followed by a 120 nm thick Au band on one edge of the network. This region was not contacted by electrolyte during electrochemical measurements.

Nafion (Aldrich) was drop-cast onto either a SWNT network or 25 μm Pt UME from a stock solution (5% wt in aliphatic alcohol/H_2O) by micro-droplet deposition[73] using a micropipet tip (Finn, Thermo Scientific) and allowed to dry under ambient conditions (Figure 1 (a)). For the SWNT samples, the resulting Nafion droplet area was measured accurately by an optical microscope (Olympus BH2). This defined the area of the SWNT–Nafion working electrode and was typically *ca*. 0.95 mm^2. The Nafion film was preconcentrated with redox-active species by soaking in an aqueous solution of 2 mM FcTMA$^+$ hexaflorophosphate (prepared in house by metathesis of ferrocenylmethyltrimethylammonium iodide, (99% Strem Chemicals) and silver hexafluorophosphate, (99% Strem Chemicals)) in 0.1 M NaCl (99.99%, Sigma Aldrich), in Milli-Q reagent grade water, for at least 18 hours. After soaking, the electrode assembly was attached to a glass microscope slide by Gel-Pak (Gel-Pak, USA), rinsed thoroughly with Milli-Q water and dried using a gentle flow of nitrogen. The thickness of films, as measured by either profilometry, micrometer or focal-plane optical microscopy, was ~100 μm. A borosilicate capillary (1.5 mm outer diameter 0.86 mm inner diameter, Clark Electromedical Instruments) containing 0.1 M NaCl and a chloridised silver wire quasi-reference counter electrode (QRCE) was positioned on the Nafion film (Figure 1 (b)) using a micrometer-equipped micropositioner (Newport). Electrical connection to the SWNT network working electrode was made by touching the gold band with a needle tipped micro-positioner (Quater Research).

Electrochemical measurements were made using a CHI 760C Bipotentiostat (CH Instruments), at room temperature (22 ± 1 °C) in an air conditioned room.

Field emission-scanning electron microscopy (FE-SEM) was performed using a Supra 55 (Zeiss). Atomic force microscopy (AFM) images were obtained in tapping mode using a Veeco Mulitmode with Nanoscope IIIa controller.

Theory and Simulations

Two models were considered, one which considered discrete site activity, [63-65, 60, 74, 75] with the remaining sidewall considered inert to the ET reaction and the second where the entire SWNT sidewall was electrochemically active.[55, 67-69] The models we develop here assume that ET is fast (reversible), which is reasonable given the fast outer sphere redox couple used (FcTMA$^{+/2+}$),[68, 69] and slow apparent diffusion rate of redox probes in Nafion (D_{app}), which is a combination of diffusion,[76] and charge transfer/electron hopping.[77] Simulations were carried out using the commercial finite element method (FEM) modelling package Comsol Multiphysics 3.3a (Comsol AB, Sweden), using the Matlab interface (Release 14) (MathWorksTM Inc., Cambridge, UK).

Discrete site activity

The locations of SWNTs on a substrate were generated randomly to provide a specified density (between 3 and 4 µm length of SWNT per µm^2 of substrate, representative of electrodes studied experimentally), with the approximation that the SWNTs were linear (Figure 2 (a (i))). With the SWNT considered inert to the electrochemical reaction, active sites ("defects") were positioned randomly on the SWNTs to provide a defect separation ranging from one defect every 100 nm (a defect density that would be uncommonly high for cCVD grown SWNTs,[69, 74] and

hence provides a generous concentration of such sites), to one defect every 4 μm (a typical value characteristic of high quality grown cCVD grown SWNTs) (Figure 2 (a(ii))).[69, 74] Note that if ET activity was confined to SWNT ends as proposed,[63, 66] the defect density would be much lower than 1 site every 4 μm, and hence this case can also be considered as a very generous (upper limit) concentration for the case where only ends are active. A Voronoi mesh for the active sites was then calculated so that the diffusional domain method could be applied[78, 79] (Figure 2 (a (iii))).

In the diffusional domain approach, the individual active sites were approximated as electrochemically active discs of radius r_1 within cylinders of radius r_2, with inert (no-flux) walls of height, h, governed by the thickness of the Nafion layer ($h = 100$ μm) (Figure 2 (b)). For each simulation, r_1 was constant, and represented the mapping of the active site onto the plane of the substrate. For each active site, r_2 was chosen so as to give an equal area to the corresponding Voronoi cell. The 2D axially symmetric geometry of a disc within a characteristic domain is shown in Figure 2 (b), with z and r being the axial and radial coordinates, respectively.

Here, we make the assumptions that the defects are of uniform size ($r_1 = 0.5$ or 1 nm), the individual diffusion domains can be approximated to a cylinder,[79, 80] and transport in the Nafion film can be described by Fick's laws of diffusion. The defect radius is assumed to be the same as the radius of a SWNT, which provides a generous approximation of the area for an active site on the sidewall. Therefore, the model provides a scenario that maximises the current from this type of reaction site. The assumption that the individual Voronoi cells can be approximated to a cylinder is valid, as long as the defect spacing is sufficiently large on the scale of the measurement so that there is relatively insignificant diffusional overlap between active sites along the same SWNT.

Model for sidewall activity

The situation where the entire sidewall of the CNT is electrochemically active was approximated by an array of parallel tubes on an insulating surface (inset of Figure 2 (c)), with the average inter-tube spacing, *w,* chosen to match the characteristic sample density. This approximation allowed the problem to be simplified to the 2D domain shown in Figure 2 (c), greatly reducing the computational time required for each simulation, compared to a full 3D model. It should be noted that this provides a somewhat idealised diffusive response as sections where the experimental SWNTs are not at the average spacing will experience diffusional overlap at different times. However for $t < 1$ s this is not a significant issue (*vide infra*).

Boundary conditions

Edge 1 represents the active site or sidewall where the following *n*-electron transfer reaction (equation 1) is considered:

$$R \rightarrow O + n e^-$$

(1)

Typically, a potential step was applied at a time, $t = 0$ s, from a value where R was not electrolysed to a potential where the conversion of species R to species O occurred at the electrode at a diffusion-controlled rate. The time-dependent diffusion equation (equation 2) was solved for species R within the interior of the domain shown by a dotted line in Figure 2 (b) and (c),[76, 81]

$$\frac{\partial c}{\partial t} = D_{app} \nabla^2 c \qquad (2)$$

where c is the concentration of species R within the Nafion film. The reaction is considered to be driven at a diffusion-limited rate at the active site, edge 1, for which the boundary condition is:

$$c = 0 \qquad (3)$$

Boundary 2 represents the electrochemically inactive Si/SiO_2 substrate and the portion of the SWNT that is inert, and was set to have zero normal flux, *i.e.*,

$$D_{app} \nabla c \cdot \mathbf{n} = 0 \qquad (4)$$

where $\mathbf{n}$ is the inward pointing unit normal vector. The diffusion domain approach dictates that there was no flux normal to boundary (3) which defined the domain and at the axis/plane of symmetry, defined by boundary (4). Boundary (5) represents the upper limit of the Nafion film where it was assumed that there was no net transfer of FcTMA$^+$ out of, or into, the film on the timescale of the experiments (equation 4). This assumption is reasonable as the experiments were completed within 60s of contacting the film with the meniscus of the pipette. The corresponding characteristic diffusion length is only ~2.1 µm (see below for determination of D_{app}), negligible compared to the overall loaded film thickness. Moreover, due to charge interactions within the Nafion film, even this is likely to represent an overestimation of any depletion that might occurr.

10

The interior of the domain enclosed by boundaries 1-5 was initially set to be at the bulk concentration, c_b, of FcTMA$^+$ in the Nafion film, as determined by experiments on the drop-cast Nafion-modified Pt UME (*vide infra*). For the discrete site activity model, equation (5) was used to calculate the current, i_s, of an individual active site,

$$i_s = 2\pi n F D_{app} \int_0^{r_1} \frac{\partial c}{\partial z} r dr \qquad (5)$$

where F is the Faraday constant. The overall current response, i, was the sum of all active sites within the simulated area (A_s). The current density with respect to the total geometric substrate area (j) was defined as:

$$j = \frac{i}{A_s} \qquad (6)$$

For the "sidewall active" model, the current density, with respect to substrate area, was defined as,

$$j = n\frac{F}{w} \int_0^L \mathbf{n.N} ds \qquad (7)$$

where L was the length of the arc of boundary 1 (Figure 2 (c)), w was the separation between nanotubes, s the arc length parameter and $\mathbf{N}$ the flux vector.

Insights from simulations

11

We consider the characteristic behaviour arising from each of the models when the heterogeneous ET reaction was driven at the diffusion-limited rate, using $D_{app} =$ 1.8 x 10^{-10} cm^2 s^{-1}, which was determined experimentally for a drop-cast Nafion film (*vide infra*). Figures 3 (a) and (b) present the development of the diffusion profile for one active site with a spacing of 360 nm (the mean value found on the most defective cCVD grown SWNTs, identified by selective electrodeposition[74]) for the discrete active site model. Even at short times (t = 0.1 ms) a hemispherical diffusion profile extends from the active site (Figure 3 (a)) and the profile is approaching a steady-state (*vide infra*). Furthermore, even after 1s, it is evident that there is negligible effect of neighbouring active sites (Figure 3 (b)), with 90% of bulk concentration reached within a distance of 4 nm (see contour) and 99% reached within 25 nm (contour not shown).

The time-dependent diffusion profile of a SWNT for the sidewall active model is significantly different. At short timescales (t = 0.1 ms), strong (hemi)cylindrical diffusion to the sidewall is observed and the SWNTs evidently behave as diffusionally-isolated elements (Figure 3 (c)). However, with time, the concentration boundary layer expands and evidently the diffusion profile starts to interact significantly with that of the neighbouring SWNT at t = 1 s (Figure 3 (d)) so that linear diffusion to the SWNT array becomes increasingly dominant on longer time scales. Note that, in the long term limit isolated tubes would be expected to behave like isolated microband or microhemicylinder electrodes, which show equivalent behaviour in the long time limit;[82] that is, they should decay with $1/(\ln(ct)$,[83, 84] where c is a constant depending on the diffusion coefficient and the width of the electrode, and not $(Dt)^{-1/2}$ which would be expected with linear diffusion.

It is clear from the time-dependent concentration profiles that the different models should produce different flux (magnitude) – time responses, and that the chronoamperometry (CA) response of the system should reflect the activity of the SWNT-Nafion composite, as we explore further below. Previously, studies of polarization curves of homogeneous (partially blocked) electrodes by Amatore *et al.* came to similar conclusions through analytical arguments.[85]

Results and Discussion

FcTMA$^+$ effective diffusion coefficient in the drop-cast Nafion film

The drop-cast Nafion film, saturated with FcTMA$^+$, was first characterised electrochemically using a 25 μm diameter Pt disc UME. The potential for the mass transport-limited oxidation of FcTMA$^+$ at the Pt-Nafion modified UME was first determined by cyclic voltammetry (CV) as shown in Figure 4 (a) for a scan rate of 100 mV s^{-1}.[29] A non-steady-state response is evident with a peak to peak separation of 190 mV.

The apparent diffusion/electron exchange coefficient of FcTMA$^+$ within the drop-cast Nafion film was then extracted using CA, by stepping the electrode potential from 0 V (where no electrode reaction occurred) to 0.5 V vs Ag/AgCl. At very long times, this tended to a steady-state limiting current (i_{lim}) of 80 pA. The *i-t* transients were analysed using the short-time expression from Shoup and Szabo,[86-89]

$$i = i_{lim} f(\tau) \tag{8}$$

where $f(\tau)$ and τ are defined by:

$$f(\tau) = 0.7854 + 0.8862\tau^{-\frac{1}{2}} + 0.2146e^{-0.7823\tau^{-\frac{1}{2}}} \qquad (9)$$

$$\tau = \frac{4D_{app}t}{a^2} \qquad (10)$$

where a is the radius of the UME. Figure 4 (b) shows a typical plot of i/i_{lim} against $t^{-1/2}$, from which $D_{app} = 1.8 \times 10^{-10}$ cm^2 s^{-1} was extracted, with a corresponding c_b value of 0.90 mol dm^{-3}. The value of D_{app} is very similar to that reported previously by Bard et al., $D_{app} = 1.7 \times 10^{-10}$ cm^2 s^{-1} for FcTMA$^+$ in drop-cast Nafion.[77]

Characterisation of SWNT samples

To compare the experimental electrochemical response of a Nafion-modified SWNT network electrode to the FEM models, the network density and size of SWNTs was needed. FE-SEM was used to measure the SWNT network density. A typical image of part of a SWNT network, Figure 5 (a), demonstrates a random distribution of SWNTs across a Si/SiO$_2$ substrate. Note that the apparent width of SWNTs observed by FE-SEM is greatly exaggerated due to charging effects. Only SWNT networks with a density in the range of 3 μm μm^{-2} to 4 μm μm^{-2} were employed as electrodes in this study. The majority of SWNTs have a height above the substrate (equivalent to SWNT diameter) between 1 nm and 2 nm, measured by AFM (Figure 5 (b) and inset).[71]

Drop-Cast Modified SWNT Networks

The driving potentials for chronoamperometric analysis were determined from a CV recorded on a Nafion modified SWNT network electrode, after saturation with

FcTMA$^+$. Figure 5 (c) shows a typical CV at a scan rate of 100 mV s^{-1} for the oxidation of FcTMA$^+$. The sigmoidal response with a quasi steady-state regime for potentials beyond 0.5 V on the forward scan indicates that, on this timescale, the regime is governed by diffusion to individual nanoscale electrode elements. Note the contrast with the data for the 25 μm diameter disc electrode (Figure 4 (a)).

The CA response for a potential step from 0 V to 0.5 V is shown in Figure 5 (d), for the SWNT-Nafion sample: prior to and after saturation with FcTMA$^+$. Comparison of the *i-t* responses indicate that the current contribution due to charging, resistive effects or other non-Faradaic processes within the film is minimal.

CA at the FcTMA$^+$ loaded SWNT-Nafion electrodes showed a linear scaling of current density (at all accessed times), when stepping to different driving potentials *i.e.* $E_{1/4}$, $E_{1/2}$, $E_{3/4}$ and the diffusion-limited potential (Figure 5 (e) and inset). This means there is essentially no change in the characteristic surface-area dependent activity of the electrode material with different driving forces. This is a particularly interesting observation which contrasts with selective metal deposition studies,[60] where the reduction of metal at SWNT surfaces was observed to occur only at discrete sites when the driving potential was low,[74] but increased in density up to contiguous nanowire formation as the driving potential was increased.[68, 74, 75, 90] This highlights a difference in the behaviour of electrodeposition systems and the classical outer-sphere ET process considered herein.

Comparison of experimental data to simulation

Figure 6 (a) shows simulated current densities for a range of average defect separations for the active site model (360 nm, 500 nm, 1 μm and 4 μm per defect).

The individual sites behave as isolated nano-disc electrodes ($t < 1$ s for a defect spacing of 360 nm to 4 μm) and provide a more-or-less steady-state and low current response on the timescale probed. The simulated steady-state response is in excellent agreement with values calculated for an array of ultramicro disc electrodes of the same size and density as the simulated active sites with no diffusional overlap.[91] As the average spacing of the active sites increases, the reported current density decreases. It is important to note, as highlighted above, that the reported current densities scale with respective overall geometric area, including the insulating substrate, hence the difference in reported current densities relates to the variation in the quantity of active material present on the surface. Figure 6 (b) demonstrates that by increasing the radius of the active sites from 0.5 nm to 1.0 nm the predicted current density increases due to the increasing area of active material on the sample. Similarly as the network density increases from 3 μm μm^{-2} to 4 μm μm^{-2} the current density for the sample increases as the number of active sites per unit area of substrate increases. The transients presented in Figure 6 (b) are all for the smallest expected average spacing of active sites on a defective SWNT (360 nm)[74] and as such represent the upper bounds for the predicted current response for defect-controlled ET activity in these networks.

The situation where the entire SWNT sidewall is active was investigated for the upper and lower bounds of SWNT network densities (3 μm μm^{-2} and 4 μm μm^{-2}) and SWNT radii (0.5 nm and 1.0 nm). Figure 6 (c) shows the calculated current density-time response for these parameters. As expected, the current density is largest for the higher density networks with the largest SWNT radius. However, in contrast to the active site model, the sidewall model provided a response of isolated nano-cylinder electrodes (for $t < 1$ s), yielding a much higher current density (as defined above) and

16

a decay of the current density with time. The many orders of magnitude difference in the simulated current densities mean that it should be possible to discriminate between the two proposed models experimentally.

Figure 6 (d) compares experimental current density-time behaviour for a SWNT network of 3.3 µm µm^{-2} with the lower and upper bounds for both the sidewall active model (red lines) and the defect only model (blue lines). Even for the case where the theoretical defect density is unfeasibly high (defect spacing 100 nm) the experimental currents are larger than predicted and order(s) of magnitude larger than for more realistic defect separations. In particular, the model for a defect spacing of 4 µm (typical of high quality SWNTs) and representing a very generous case where ends only are active predicts a current density that is 3 orders of magnitude smaller than seen experimentally. This leaves the case where SWNTs sidewalls are completely active for us to consider.

Figure 6 (d) shows that the experimental data (solid line), while in better agreement with the sidewall active model, is lower than simulated for an entirely active parallel array of SWNTs. There are several likely factors for the difference: (1) the parallel SWNT model of equivalent density to a random SWNT network will tend to overestimate the current density. (2) The Nafion film may not fully wet all of the SWNTs, resulting in a reduced area of SWNT in contact with the electrolyte. (3) We have shown recently that not all SWNTs are active in networks resulting in a smaller active network density than estimated by AFM imaging.[68, 69] The latter point is supported by differences in electroactivity between SWNTs that have been observed using metal deposition on cCVD grown SWNTs,[60, 74] where some SWNTs were found not to support metal deposition, and display quasi-insulator properties, which was

attributed to poor conductivity or connectivity of individual SWNTs within the network.[60, 74] This has been further confirmed with recent SECCM studies.[69]

Conclusions

We have investigated quantitatively the intrinsic electrochemical activity of SWNT-Nafion composites using a drop-cast Nafion film on a SWNT network. Using UME chronoamperometry, the apparent diffusion coefficient of a redox probe, FcTMA$^+$, within the Nafion film was determined as 1.8×10^{-10} cm^2 s^{-1}, together with a saturated concentration of 0.9 M. The arrangement described is attractive for fundamental studies because the small diffusion coefficient of the redox probe, together with the relatively sparse density of SWNTs in the 2-D network, mean that characteristic sites for ET become spatially decoupled on the voltammetric timescale. We have thus been able to use FEM modelling to assess candidate activity models for the cases where: (i) the activity is confined to sites on the sidewall at a density consistent with literature values;[74] and (ii) the SWNTs are completely active and represented by a parallel SWNT array of equivalent density. The former case predicted current densities that are orders of magnitude smaller than observed experimentally, suggesting that SWNTs have substantially higher activity. On the other hand, the case where all SWNTs are fully active predict a current density that is too high, indicating that some SWNTs in the network are highly resistive and not fully connected in the network (consistent with direct measurements on unmodified SWNTs[68, 69]) and/or that not all SWNTs are fully wetted by Nafion. The latter would be expected, at least in part, because Nafion films can be considered as an array of cylindrical water nanochannels with diameters and spacings that are slightly larger

than the SWNTs used herein.[92] This nanostructuring would reasonably be expected to slightly diminish the area of SWNTs accessible to the redox mediator.

**Acknowledgements**

References

1.   S. Hrapovic, Y. Liu, K. B. Male and J. H. T. Luong, *Anal. Chem.*, 2003, **76**, 1083-1088.
2.   Y. C. Tsai, J. M. Chen and F. Marken, *Microchim. Acta*, 2005, **150**, 269-276.
3.   M. Zhang and W. Gorski, *J. Am. Chem. Soc.*, 2005, **127**, 2058-2059.
4.   V. Khomenko, E. Frackowiak and F. Béguin, *Electrochim. Acta*, 2005, **50**, 2499-2506.
5.   P. P. Joshi, S. A. Merchant, Y. Wang and D. W. Schmidtke, *Anal. Chem.*, 2005, **77**, 3183-3188.
6.   N. G. Sahoo, S. Rana, J. W. Cho, L. Li and S. H. Chan, *Prog. Polym. Sci.*, 2010, **35**, 837-867.
7.   K. A. Mauritz and R. B. Moore, *Chem. Rev.*, 2004, **104**, 4535-4586.
8.   F.-H. Wu, G.-C. Zhao and X.-W. Wei, *Electrochem. Commun.*, 2002, **4**, 690-694.
9.   Z. Guo and S. Dong, *Anal. Chem.*, 2004, **76**, 2683-2688.
10.   J. Li, S. Guo, Y. Zhai and E. Wang, *Electrochem. Commun.*, 2009, **11**, 1085-1088.
11.   H. Xu, L. Zeng, S. Xing, Y. Xian and G. Shi, *Electroanal.*, 2008, **20**, 2655-2662.
12.   L. S. Rocha and H. M. Carapuca, *Bioelectrochemistry*, 2006, **69**, 258-266.
13.   B. J. Sanghavi and A. K. Srivastava, *Electrochim. Acta*, 2011, **56**, 4188-4196.
14.   R. Kannan, B. A. Kakade and V. K. Pillai, *Angew. Chem.-Int. Edit.*, 2008, **47**, 2653-2656.
15.   B. Rajesh, V. Karthik, S. Karthikeyan, K. R. Thampi, J. M. Bonard and B. Viswanathan, *Fuel*, 2002, **81**, 2177-2190.
16.   W. Li, X. Wang, Z. Chen, M. Waje and Y. Yan, *J. Phys. Chem. B*, 2006, **110**, 15353-15358.
17.   B. Smitha, S. Sridhar and A. A. Khan, *J. Membr. Sci.*, 2005, **259**, 10-26.
18.   V. Tricoli, N. Carretta and M. Bartolozzi, *J. Electrochem. Soc.*, 2000, **147**, 1286-1290.
19.   S. J. Lee, S. Mukerjee, J. McBreen, Y. W. Rho, Y. T. Kho and T. H. Lee, *Electrochim. Acta*, 1998, **43**, 3693-3701.
20.   B. Rajesh, K. Ravindranathan Thampi, J. M. Bonard, N. Xanthopoulos, H. J. Mathieu and B. Viswanathan, *J. Phys. Chem. B*, 2003, **107**, 2701-2708.
21.   T. P. Henning and A. J. Bard, *J. Electrochem. Soc.*, 1983, **130**, 613-621.
22.   T. P. Henning, H. S. White and A. J. Bard, *J. Am. Chem. Soc.*, 1982, **104**, 5862-5868.
23.   M. Krishnan, J. R. White, M. A. Fox and A. J. Bard, *J. Am. Chem. Soc.*, 1983, **105**, 7002-7003.
24.   T. P. Henning, H. S. White and A. J. Bard, *J. Am. Chem. Soc.*, 1981, **103**, 3937-3938.
25.   P. Bertoncello, M. K. Ram, A. Notargiacomo, P. Ugo and C. Nicolini, *Phys. Chem. Chem. Phys.*, 2002, **4**, 4036-4043.
26.   F. C. Anson, Y. M. Tsou and J. M. Saveant, *J. Electroanal. Chem.*, 1984, **178**, 113-127.
27.   D. A. Buttry and F. C. Anson, *J. Am. Chem. Soc.*, 1982, **104**, 4824-4829.
28.   D. A. Buttry and F. C. Anson, *J. Am. Chem. Soc.*, 1984, **106**, 59-64.

29. M. Pyo and A. J. Bard, *Electrochim. Acta*, 1997, **42**, 3077-3083.
30. P. Bertoncello, I. Ciani, F. Li and P. R. Unwin, *Langmuir*, 2006, **22**, 10380-10388.
31. K. P. Gong, Y. Dong, S. X. Xiong, Y. Chen and L. Q. Mao, *Biosens. Bioelectron.*, 2004, **20**, 253-259.
32. X. Liu, L. Shi, W. Niu, H. Li and G. Xu, *Biosens. Bioelectron.*, 2008, **23**, 1887-1890.
33. H. Tang, J. H. Chen, S. Z. Yao, L. H. Nie, G. H. Deng and Y. F. Kuang, *Anal. Biochem.*, 2004, **331**, 89-97.
34. D. R. S. Jeykumari, S. Ramaprabhu and S. S. Narayanan, *Carbon*, 2007, **45**, 1340-1353.
35. C. R. Raj and S. Chakraborty, *Biosens. Bioelectron.*, 2006, **22**, 700-706.
36. Y. Cao, R. Yuan, Y. Chai, L. Mao, X. Yang, S. Yuan, Y. Yuan and Y. Liao, *Electroanal.*, 2011, **23**, 1418-1426.
37. S. Chen, R. Yuan, Y. Chai, L. Min, W. Li and Y. Xu, *Electrochim. Acta*, 2009, **54**, 7242-7247.
38. P.-Y. Chen, R. Vittal, P.-C. Nien and K.-C. Ho, *Biosens. Bioelectron.*, 2009, **24**, 3504-3509.
39. H.-S. Wang, T.-H. Li, W.-L. Jia and H.-Y. Xu, *Biosens. Bioelectron.*, 2006, **22**, 664-669.
40. K. B. Wu and S. S. Hu, *Microchim. Acta*, 2004, **144**, 131-137.
41. M. E. Rice, A. F. Oke, C. W. Bradberry and R. N. Adams, *Brain Res.*, 1985, **340**, 151-155.
42. J. A. Ni, H. X. Ju, H. Y. Chen and D. Leech, *Anal. Chim. Acta*, 1999, **378**, 151-157.
43. J. Maruyama and I. Abe, *Electrochim. Acta*, 2001, **46**, 3381-3386.
44. A. Jarzebinska, P. Rowinski, I. Zawisza, R. Bilewicz, L. Siegfried and T. Kaden, *Anal. Chim. Acta*, 1999, **396**, 1-12.
45. L. M. Moretto, T. Kohls, A. Chovin, N. Sojic and P. Ugo, *Langmuir*, 2008, **24**, 6367-6374.
46. P. Bertoncello, L. Dennany, R. J. Forster and P. R. Unwin, *Anal. Chem.*, 2007, **79**, 7549-7553.
47. P. Bertoncello, A. Notargiacomo and C. Nicolini, *Langmuir*, 2005, **21**, 172-177.
48. P. Bertoncello and P. Ugo, *J. Braz. Chem. Soc.*, 2003, **14**, 517-522.
49. J. Wang, M. Musameh and Y. H. Lin, *J. Am. Chem. Soc.*, 2003, **125**, 2408-2409.
50. M. A. Edwards, P. Bertoncello and P. R. Unwin, *J. Phys. Chem. C*, 2009, **113**, 9218-9223.
51. I. Rubinstein and A. J. Bard, *J. Am. Chem. Soc.*, 1980, **102**, 6641-6642.
52. I. Rubinstein and A. J. Bard, *J. Am. Chem. Soc.*, 1981, **103**, 5007-5013.
53. Y. C. Tsai, S. C. Li and J. M. Chen, *Langmuir*, 2005, **21**, 3653-3658.
54. Z. Lin, J. Chen and G. Chen, *Electrochim. Acta*, 2008, **53**, 2396-2401.
55. I. Heller, J. Kong, A. Hendrik, H. A. Heering, K. A. Williams, S. G. Lemay and C. Dekker, *Nano Lett.*, 2005, **5**, 137-142.
56. I. Dumitrescu, P. R. Unwin, N. R. Wilson and J. V. Macpherson, *Anal. Chem.*, 2008, **80**, 3598-3605.
57. P. Bertoncello, J. P. Edgeworth, J. V. Macpherson and P. R. Unwin, *J. Am. Chem. Soc.*, 2007, **129**, 10982-10983.

58. I. Dumitrescu, J. P. Edgeworth, P. R. Unwin and J. V. Macpherson, *Adv. Mater.*, 2009, **21**, 3105-3109.
59. S. Rosenblatt, Y. Yaish, J. Park, J. Gore, V. Sazonova and P. L. McEuen, *Nano Lett.*, 2002, **2**, 869-872.
60. T. M. Day, P. R. Unwin, N. R. Wilson and J. V. Macpherson, *J. Am. Chem. Soc.*, 2005, **127**, 10639-10647.
61. B. M. Quinn, C. Dekker and S. G. Lemay, *J. Am. Chem. Soc.*, 2005, **127**, 6146-6147.
62. I. Dumitrescu, P. R. Unwin and J. V. Macpherson, *Chem. Commun.*, 2009, **45**, 6886-6901.
63. C. E. Banks, R. R. Moore, T. J. Davies and R. G. Compton, *Chem. Commun.*, 2004, **16**, 1804-1805.
64. A. F. Holloway, K. Toghill, G. G. Wildgoose, R. G. Compton, M. A. H. Ward, G. Tobias, S. A. Llewellyn, B. n. Ballesteros, M. L. H. Green and A. Crossley, *J. Phys. Chem. C*, 2008, **112**, 10389-10397.
65. A. Chou, T. Bocking, N. K. Singh and J. J. Gooding, *Chem. Commun.*, 2005, **7**, 842-844.
66. C. E. Banks, T. J. Davies, G. G. Wildgoose and R. G. Compton, *Chem. Commun.*, 2005, **7**, 829-841.
67. J. Kim, H. Xiong, M. Hofmann, J. Kong and S. Amemiya, *Anal. Chem.*, 2010, **82**, 1605-1607.
68. P. V. Dudin, M. E. Snowden, J. V. Macpherson and P. R. Unwin, *ACS Nano*, 2011, **5**, 10017-10025.
69. A. G. Güell, N. Ebejer, M. E. Snowden, K. McKelvey, J. V. Macpherson and P. R. Unwin, *Proc. Natl. Acad. Sci. U. S. A.*, 2012, **109**, 11487-11492.
70. E. Garcia, J. Kwak and A. J. Bard, *Inorg. Chem.*, 1988, **27**, 4377-4382.
71. J. P. Edgeworth, N. R. Wilson and J. V. Macpherson, *Small*, 2007, **3**, 860-870.
72. E. S. Snow, J. P. Novak, P. M. Campbell and D. Park, *Appl. Phys. Lett.*, 2003, **82**, 2145-2147.
73. A. Lutfurakhmanov, G. K. Loken, D. L. Schulz and I. S. Akhatov, *Appl. Phys. Lett.*, 2010, **97**, 124107-124103.
74. Y. W. Fan, B. R. Goldsmith and P. G. Collins, *Nature Mater.*, 2005, **4**, 906-911.
75. T. M. Day, P. R. Unwin and J. V. Macpherson, *Nano Lett.*, 2007, **7**, 51-57.
76. A. J. Bard and L. R. Faulkner, *Electrochemical Methods*, John Wiley and Sons, New York, 2001.
77. H. S. White, J. Leddy and A. J. Bard, *J. Am. Chem. Soc.*, 1982, **104**, 4811-4817.
78. T. J. Davies, S. Ward-Jones, C. E. Banks, J. del Campo, R. Mas, F. X. Munoz and R. G. Compton, *J. Electroanal. Chem.*, 2005, **585**, 51-62.
79. T. J. Davies and R. G. Compton, *J. Electroanal. Chem.*, 2005, **585**, 63-82.
80. T. J. Davies, R. R. Moore, C. E. Banks and R. G. Compton, *J. Electroanal. Chem.*, 2004, **574**, 123-152.
81. C. M. A. Brett and A. M. O. Brett, *Electrochemistry Principles*, Oxford Press, Oxford, 1993.
82. C. A. Amatore, B. Fosset, M. R. Deakin and R. M. Wightman, *J. Electroanal. Chem.*, 1987, **225**, 33-48.
83. D. Britz, K. Poulsen and J. Strutwolf, *Electrochim. Acta*, 2005, **51**, 333-339.
84. K. Aoki, K. Tokuda and H. Matsuda, *J. Electroanal. Chem.*, 1987, **225**, 19-32.

85. C. Amatore, J. M. Saveant and D. Tessier, *J. Electroanal. Chem.*, 1983, **147**, 39-51.
86. D. Shoup and A. Szabo, *J. Electroanal. Chem.*, 1982, **140**, 237-245.
87. C. P. Winlove, K. H. Parker and R. K. C. Oxenham, *J. Electroanal. Chem.*, 1984, **170**, 293-304.
88. M. V. Mirkin, F.-R. F. Fan and A. J. Bard, *J. Electroanal. Chem.*, 1992, **328**, 47-62.
89. J. V. Macpherson and P. R. Unwin, *Anal. Chem.*, 1997, **69**, 2063-2069.
90. N. R. Wilson and D. H. Cobden, *Nano Lett.*, 2008, **8**, 2161-2165.
91. W. E. Morf and N. F. de Rooij, *Sensors and Actuators B:Chemical*, 1997, **44**, 538-541.
92. K. Schmidt-Rohr and Q. Chen, *Nature Mater.*, 2008, **7**, 75-83.
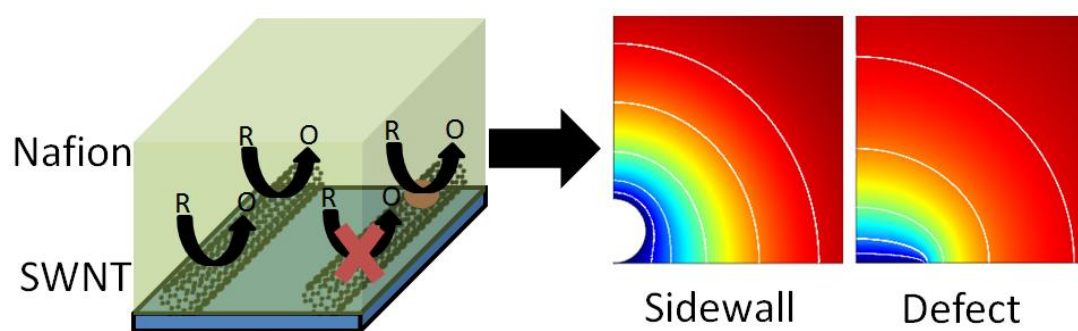
A combination of experiment and numerical modelling reveals the characteristic electrochemical activity of single walled nanotube (SWNT)-Nafion assemblies
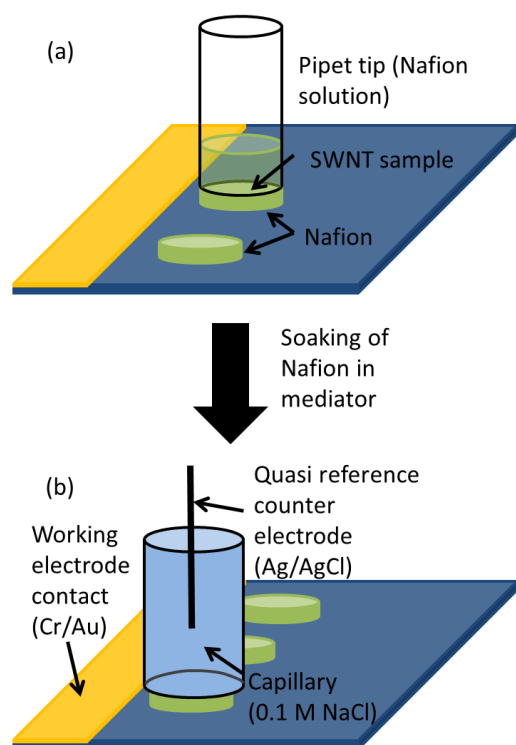
Figures

Figure 1. Schematic of part of the experimental procedure showing: (a) deposition of Nafion by micro droplet deposition prior to preconcentration with FcTMA$^+$. (b) The electrochemical setup for measurements on loaded drop cast Nafion films. Not to scale.
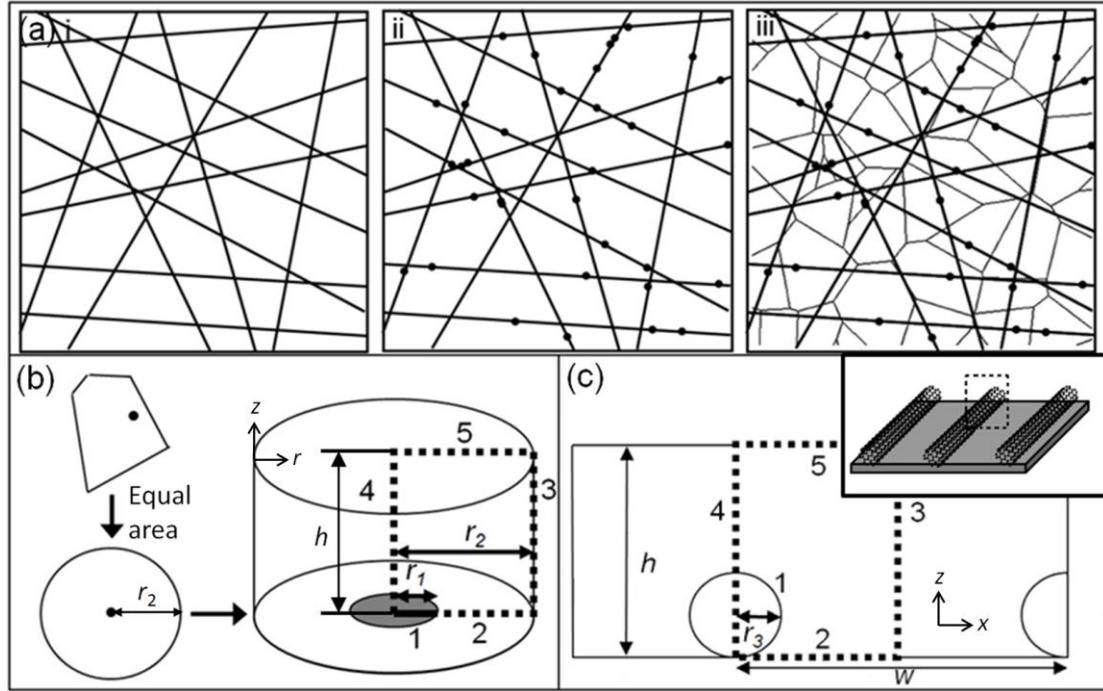
Figure 2. (a) Schematic to show the calculation of Voronoi cells for the active site model. (i) Straight CNTs were placed randomly to generate the network, (ii) active sites were placed randomly along the CNTs at the desired average defect spacing, (iii) Voronoi cells were calculated for the active sites. (b) Translation of a Voronoi cell to an isolated active disc of radius r_1 within an insulating cylinder of radius r_2, where r_2 was chosen to give equal area to the Voronoi cell. (c) The 2D repeating unit used in the "sidewall active" model is outlined by the dotted line, where r_3 is the CNT radius and w is the average spacing of the CNTs. The inset shows a 3D representation of parallel CNTs. Figures not to scale.
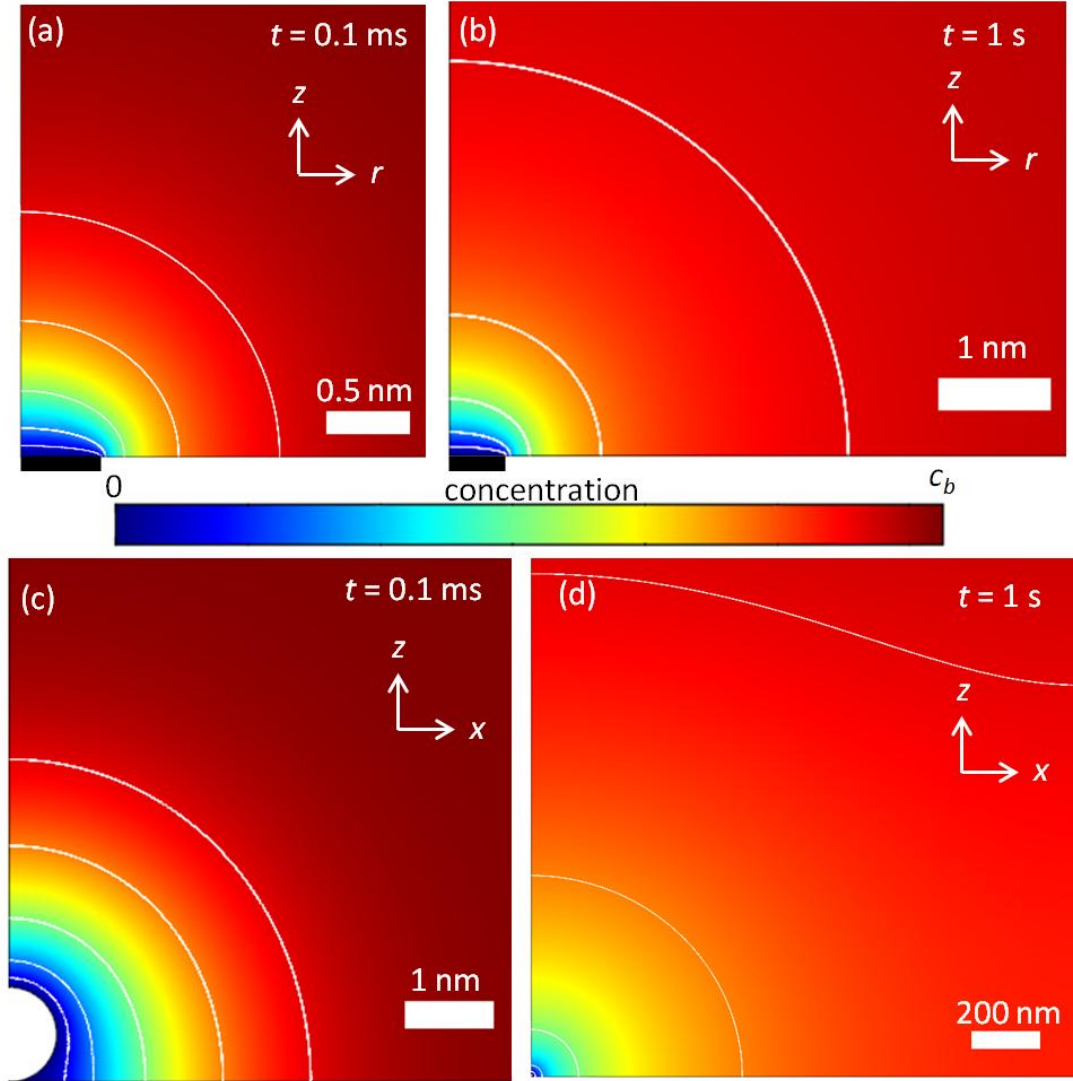
Figure 3. Concentration profiles from FEM simulations illustrating the expansion of the diffusion layer with time for different cases. The profiles in (a) and (b) show results of the active site model with a site of radius 0.5 nm and average spacing of 360 nm at times 0.1 ms and 1 s, respectively. The profiles in (c) and (d) are results from the sidewall active model for a SWNT of radius 0.5 nm in a network of density 3 μm μm^{-2} at times of 0.1 ms and 1 s. Contour lines represent $c = 0.1c_b$, $0.25c_b$, $0.5c_b$, $0.75c_b$, and $0.9c_b$ respectively. Defect sites are illustrated by black bars.
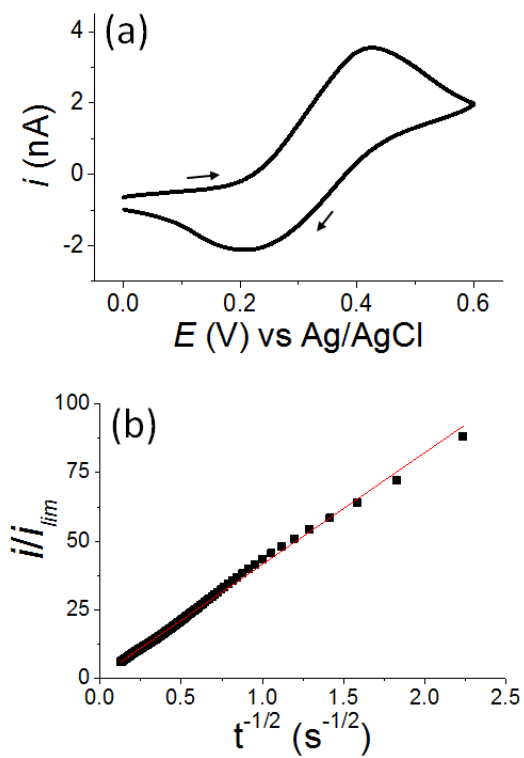
Figure 4. Oxidation of FcTMA^{+} in a Nafion-coated 25 μm diameter Pt UME. (a) CV at 100 mV s^{-1}; (b) i/i_{lim} vs $t^{-1/2}$ (experimental points and solid line of best fit to eq. 8) for the diffusion-limited oxidation of FcTMA^{+}.
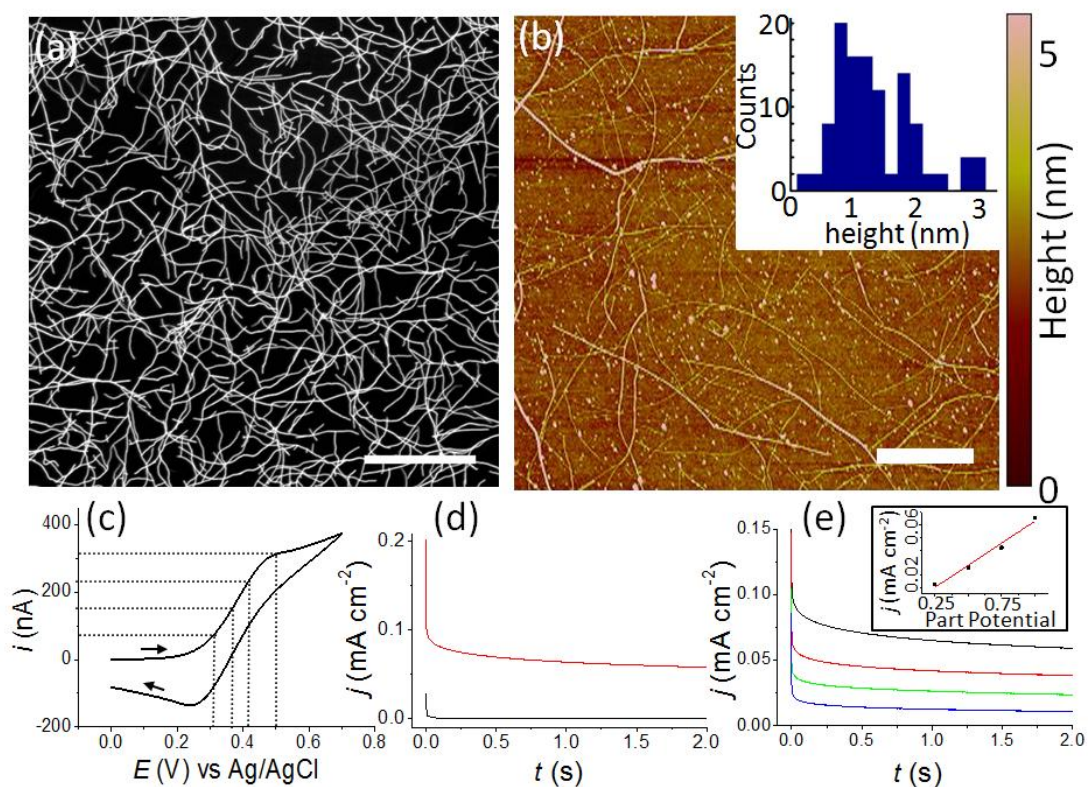
Figure 5. (a) FE-SEM image of a typical SWNT sample (scale bar 6 μm). (b) AFM of a SWNT network electrode (scale bar 1 μm) representative of a network of density 3.4 μm μm^{-2}. Inset is a histogram of SWNT heights. (c) Cyclic voltammetry at 100 mV s^{-1} of drop-cast Nafion on SWNT network saturated with FcTMA$^+$. Lines show relative positions of $E_{1/4}$, $E_{1/2}$, $E_{3/4}$ and a diffusion-limited potential. (d) CA at the diffusion-limited potential for FcTMA$^+$ oxidation at a SWNT network electrode sample with drop-cast Nafion film with no FcTMA$^+$ (black line) and saturated with FcTMA$^+$ (red line). (e) CA of drop-cast Nafion on a SWNT network saturated with FcTMA$^+$ at $E_{1/4}$ (blue line), $E_{1/2}$ (green line), $E_{3/4}$ (red line), and the diffusion-limited potential (black line) showing linear scaling between the different driving potentials (inset at $t = 1$ s, a part potential of 0.25 refers to $E_{1/4}$ and a part potential of 0.75 refers to $E_{3/4}$).
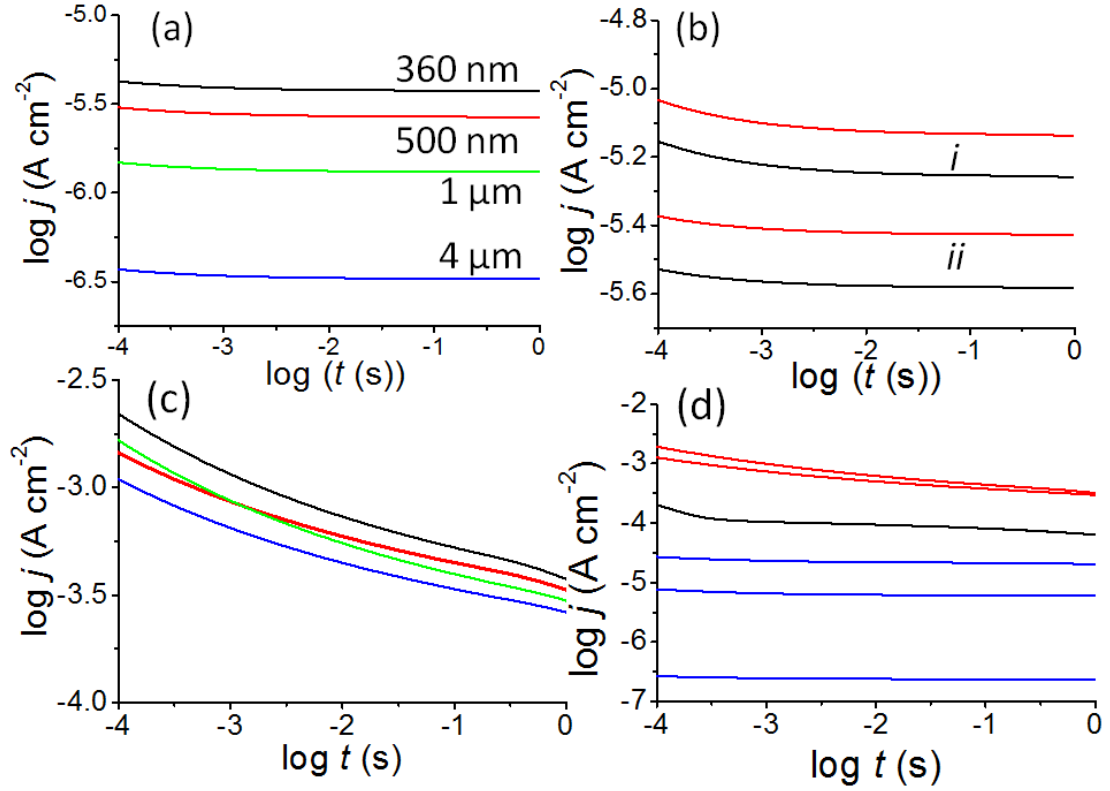
Figure 6. Simulated current density - time data for different parameters of the discrete active site model, where (a) the effect of changing the average defect spacing for a network of density 4 μm μm^{-2} with defect radii of 0.5 nm is shown. (b) The dependence of the current density on the network density and size of defect, for network densities of 3 (black line) and 4 μm μm^{-2} (red line) and for defect radii of (i) 1 nm and (ii) 0.5 nm. Average defect spacing 360 nm. (c) Simulated current density – time dependence for the sidewall active model on the network density and radius of the SWNT, with a network density of 4 μm μm^{-2} and SWNTs radii of 1 nm (black line) and 0.5 nm (red line); and a network density of 3 μm μm^{-2} with SWNT radii of 1 nm (green line) and 0.5 nm (blue line). (d) The upper and lower current density bounds for (i) the sidewall active model (red lines: 1 nm radius upper, 0.5 nm radius lower) and (ii) the discrete active site model, where the blue lines indicate defect spacing of 100 nm (highest current density), 360 nm and 4 μm (lowest current density), for a SWNT radius of 1 nm. Black solid line is experimental data. All data are for a SWNT network of density 3.3 μm μm^{-2}.